Biochimica et Biophysica Acta 1840 (2014) 2331–2339

Contents lists available at ScienceDirect

Biochimica et Biophysica Acta

journal homepage: www.elsevier.com/locate/bbagen

Tracing the pathway of compositional changes in bone mineral with age: Preliminary study of bioapatite aging in hypermineralized dolphin's bulla

Zhen Li, Jill D. Pasteris *

Department of Earth and Planetary Sciences, Washington University in St. Louis, St. Louis, MO 63130, USA

ARTICLE INFO

Article history:
Received 7 January 2014
Received in revised form 7 March 2014
Accepted 11 March 2014
Available online 17 March 2014

Keywords:
Bulla
Aging
Hypermineralization
Bone mineral
Carbonated hydroxylapatite

ABSTRACT

Background: Studies of mineral compositional effects during bone aging are complicated by the presence of collagen.
Methods: Hypermineralized bullae of Atlantic bottlenose dolphins of <3 months, 2.5 years, and 20 years underwent micrometer-scale point analysis by Raman spectroscopy and electron microprobe in addition to bulk analysis for carbon.
Results: Bulla central areas have a mineral content of ~96 wt.% and 9–10 wt.% carbonate in their bioapatite, which is ~2 wt.% more than edge areas. Ca/P atomic ratios (~1.8) and concentrations of Mg, S, and other minor/trace elements are almost constant in central areas over time. Maturity brings greater over-all homogeneity in mineral content, stoichiometry, and morphology throughout the central and edge areas of the bullae. During aging, edge areas become less porous, whereas the concentration of organics in the edge is reduced. Enhancement of coupled substitutions of CO_3^{2-} for PO_4^{3-} and Na for Ca during aging increases carbonate content up to ~10 wt.% in the adult bulla.
Conclusions: 1) Changes in physical properties during aging did not occur simultaneously with changes in chemical properties of the bone mineral. 2) Compositional changes in bone mineral were minor during the neonatal to sub-adult stage, but significant during later maturity. 3) Na and CO_3 concentrations co-vary in a 1:1 molar proportion during aging. 4) The mineral's crystallinity did not decrease as CO_3 concentration increased during aging.
General significance: Hypermineralized dolphin's bulla, due to extreme depletion in collagen, is an ideal material for investigating mineralogical changes in bioapatite during bone aging.

1. Introduction

Hypermineralized bone materials reveal much about the nature of the mineral component of bone. The dolphin's ear bone (bulla) is remarkable due to its extreme density (~2.5 g/cm^3 in adults) and mineral content (reported to be ~85 wt.% in adults) [1,2], which make it one of the most hypermineralized bone materials recognized. In addition, dolphins have a lifespan over 40 years, which is much longer than many animal models typically used in bone research, e.g., rat, rabbit, and pig. The bullae in dolphins therefore were selected as especially appropriate for the study of an ontogenetic sequence of bone mineral that could have clinical relevance for humans.

The bulla is one of the most addressed subjects in the literature on dolphins [2–5]. It is believed to improve the efficiency of ultrasound conduction and/or to enhance the bilateral discrimination of sound direction undersea [3,6]. The bulla resides in an extensive peribullar cavity outside the skull and differs from temporal bone complexes of other mammals, such as humans, in its construction, position, and possibly function [3]. It consists of two connected parts, called the "tympano-periotic complex". The periotic bulla is dorsal and slightly medial to the shell-like tympanic bulla.

The bulla is hypermineralized even in neonates, and the mineral content can reach its maximum at 6 months [1]. The mineral in the bulla, as in normal bone (i.e., that which contains sub-equal volumes of mineral and collagen) and tooth, is biologically precipitated apatite. Bioapatite is a form of carbonated hydroxylapatite (CHAP) with an approximate formula of [7–9]

$$(Ca)_{10-x}[(PO_4)_{6-x}(CO_3)_x](OH)_{2-x}\cdot 1.5H_2O. \quad (1)$$

Bioapatite is usually non-stoichiometric due to both hydroxyl- and calcium-deficiency [10], which are coupled with the carbonate substitution as shown in Formula (1). Most of the carbonate substitutes for phosphate in bone mineral, although 10–15% of the carbonate substitutes for OH^- ions in channels within the mineral [11]. A normal bone contains 5–8 wt.% carbonate [12,13]. However, the bioapatite in the dolphin's bulla is reported to have a very high carbonate content of ~9 wt.% [14], even higher than the ~8 wt.% in other whales' bullae and the rostrum of the *Mesoplodon densirostris* (MD) whale [15].

In normal bone, the average mineral content increases with maturity [16,17]. Several studies show increased carbonate and some amount of

* Corresponding author. Tel.: +1 314 935 5434; fax: +1 314 935 7361.
E-mail address: pasteris@levee.wustl.edu (J.D. Pasteris).

http://dx.doi.org/10.1016/j.bbagen.2014.03.012
0304-4165/

increase of crystallite size with age [16–23]. It has been documented that water concentration in living bone and in its mineral decreases with bone maturity [19,24–26]. There is also evidence that the proportion of carbonate residing in the channel sites (rather than substituting for phosphate) increases with the bone's age [19,24], i.e., as water concentration decreases. However, many of the measurements made on normal bone are hindered by the high concentration of collagen in bone (~40 wt.% collagen and 10–15 wt.% water), which is a limitation that this study attempts to remedy.

Hypermineralized bone provides another approach to study the aging effects in bone. The current work is a preliminary study on mineralogical changes in the bullae with maturity. In spite of the long history of Cetacean research, the mineralogy of the bioapatite in the dolphin's bulla has not been documented in detail. Mineralogical changes in the bulla during aging, e.g., carbonate content, cation (Ca, Mg, and Na) concentrations, and degree of crystallinity, are still unknown. In the present study, Raman spectroscopy, carbon analysis, and electron microprobe analysis were applied to investigate the bullae of the most studied whale species — the Atlantic bottlenose dolphin (*Tursiops truncates*, TT).

2. Materials and methods

2.1. Materials

Samples of dolphins' bullae are not rare, but obtaining fresh bullae appropriate for medical research requires timely collection from carcasses near coasts. Therefore, it is difficult to obtain multiple series of bulla samples at known, appropriately separated age. Fortunately, previous histological studies of dolphin bullae have shown that such mineralogical features as mineral content are almost identical among different bullae of the same age and that they change at an extremely slow rate [1]. Therefore, three bullae of TT dolphins with an overall age range of 20 years were obtained from the Department of Vertebrate Zoology of the Smithsonian Institution in Washington, D.C., for this pilot study. Samples from TT dolphins at specific maturity levels were selected, i.e., neonate (USNM#504398, 116 cm), sub-adult (USNM#504400, 196 cm), and adult (USNM#504121, 249 cm). The host animals' estimated ages, based on the body length [27], are <3 months for the neonate, 2.5 years for the sub-adult, and 20 years for the adult. It has been recognized that tympanic and periotic bones share similar mineralogic and histologic features [1]. Furthermore, part of the periotic bone of the adult TT was missing, as received (as is common in collections of whale and dolphin bullae). Therefore, the tympanic bullae were selected for comparative analysis in the present study.

Each tympanic bulla sample was sawn across the mid-shaft using an Isomet low-speed diamond saw (Buehler Ltd., Lake Bluff, IL) for preparation of thin sections (see Fig. 1). The midshaft slices were then cut into two thinner wafers (with equal thickness of about 3 mm): one wafer was pulverized into powder for carbon analyses; the second wafer was ground and well-polished into 30 μm-thick transverse sections (prepared by Applied Petrographic Services, Inc., Greensburg, PA) for optical microscopy, Raman spectroscopy, and electron microprobe studies. The latter three types of analyses were carried out on chemically untreated material. All analyses were performed on involucra (major part of tympanic bulla). None of the materials in the present study underwent histologic staining or chemical preservation.

2.2. Instrumentation

Raman microprobe spectroscopy was applied to observe vibrational modes to characterize the sample materials. It was performed with a fiber-optically coupled Raman microprobe (HoloLab Series 5000 Raman Microprobe, Kaiser Optical System, Inc.). The spectral region of 100–4000 cm^{-1} was recorded using 532 nm excitation at 10 mW laser power (excitation delivered by a frequency-doubled Nd:YAG laser). The diameter of the focused laser spot was 1 μm for all Raman spectra. The typical acquisition was 32 × 4 s per analysis spot using an MSPlan 80× objective, N.A. = 0.85 (Olympus, Japan).

Total carbon (TC) and carbon associated with the mineral, i.e., total inorganic carbon (TIC), were analyzed in a CM5015 CO_2 coulometer (UIC Inc.) at the University of Kansas, Manhattan, KS. TC was determined by combusting the rostrum sample in a tube furnace at 950 °C and then measuring the evolved CO_2 in a coulometric titration cell. TIC was determined by adding perchloric acid to the sample and then measuring the evolved CO_2 gas. The details of the sample preparation and data acquisition have been reported [28–30]. Organic carbon (TOC) was calculated by the difference: TOC = TC − TIC.

Electron microprobe (EMP) analysis was performed with a JEOL JXA 8200 Superprobe. Carbon-coated polished sections were studied with an accelerating voltage of 15 kV. Quantitative point analysis was accomplished with a beam current of 25 nA and a beam diameter of 20 μm. The elements F, Ca, P, Na, Mg, S, K, and Cl were selected for quantitative analysis by wavelength-dispersive X-ray spectroscopy (WDS). The calibration standards for the EMP analyses were naturally occurring geological mineral samples that included Durango apatite for Ca, P, and F, albite for Na, synthetic forsterite for Mg, anhydrite for S, microcline for K, and tugtupite for Cl. In addition, back-scattered-electron (BSE) images were taken at an accelerating voltage of 15 kV to evaluate chemical homogeneity of the sections.

3. Results

3.1. Microscopy and Raman spectroscopy

In the original, unsawn samples, the three TT bullae show similar lengths (3.4–3.5 cm) of tympanic bone (Fig. 1). However, the involucrum of the neonate TT is visibly thinner than those of the sub-adult and adult (see vertical height in Fig. 2). The neonate tympanic bone shows a more porous texture on its surface compared to the sub-adult and adult samples (see Fig. 1). A comparison of transverse thin-

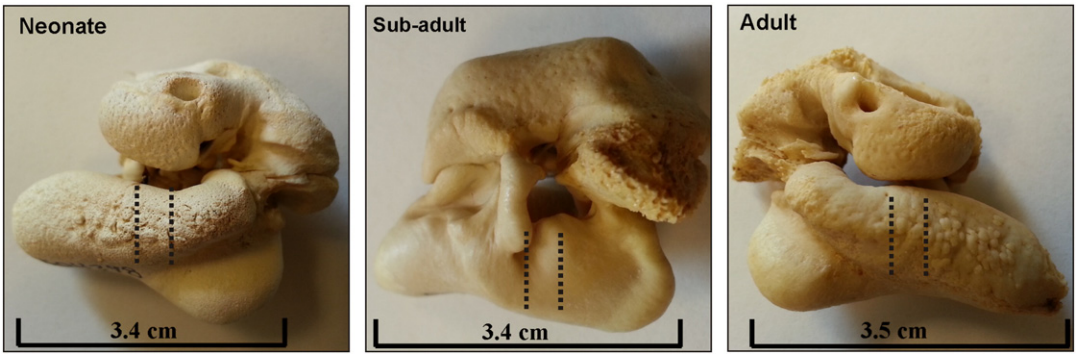

Fig. 1. Images of neonate, sub-adult, and adult TT bullae (tympano-periotic complex). Dashed lines indicate volumes of tympanic bone cut for making transverse polished thin-sections.

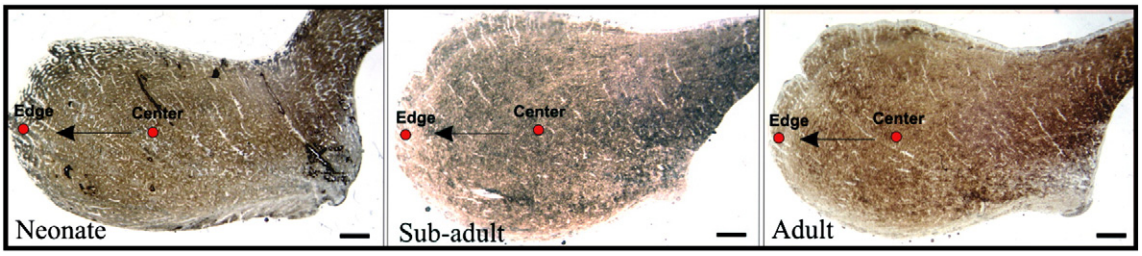

Fig. 2. Images of three TT transverse sections in transmitted, plane-polarized light (scale bar = 1 mm). Marked edge and center spots on the involucra of the tympanic bullae are positions studied by Raman spectroscopy.

sections confirms the abundant porosity in the neonate tympanic bone, especially on the edges of the section (Fig. 2). There is no apparent difference in texture between the sub-adult and adult sections, either in the central (dominant) areas or in the narrow edge areas.

Raman spectroscopy was performed on central (dominant) regions and on the outermost edge areas in transverse sections of the three TT involucra (see Fig. 2). The most intense peak for the mineral phase in all samples is the ν_1P–O symmetric stretch at ~960 cm^{-1}, which together with its other peaks confirm the phosphate phase in all samples to be apatite [13,31–33]. Dominant areas, e.g., central spots in all three sections, show similar Raman spectra (Fig. 3, upper three spectra in A). Edge areas of all three sections show spectra similar to each other (Fig. 3, bottom three spectra in A), but have peaks in addition to those for apatite (Fig. 3, bottom three spectra in B).

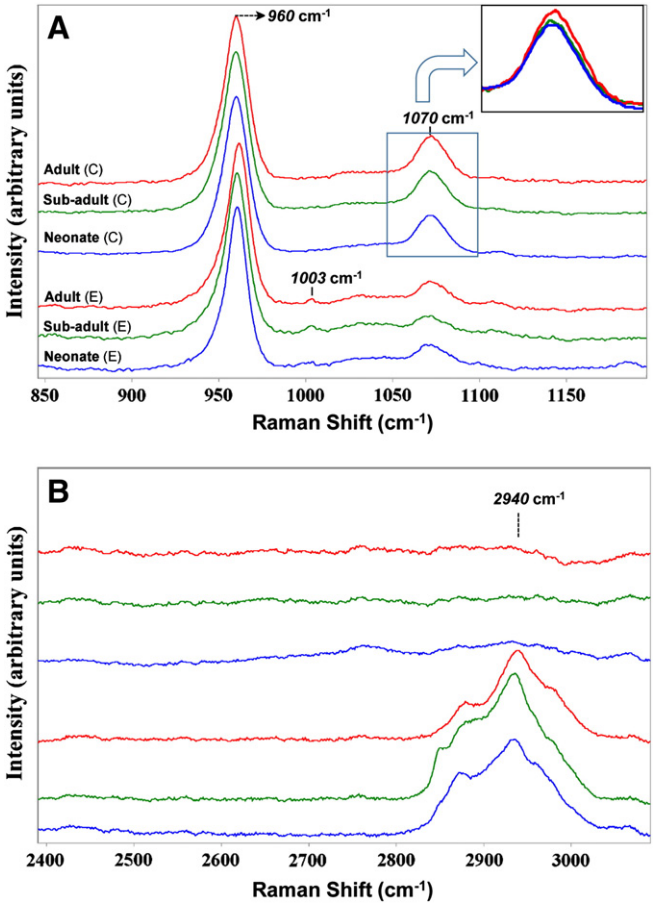

Fig. 3. Raman spectra on transverse sections of neonate, sub-adult, and adult TT bullae (all spectra were normalized to the intensity of the 960 cm^{-1} peak). Spectra in central areas (C) and edges (E) of the three samples are shown. A: 850–1200 cm^{-1} region shows major peaks of carbonate (1070 cm^{-1}) and phosphate (960 cm^{-1}). Upper right inset is a stack of normalized 1070 cm^{-1} peaks indicating relative carbonate concentration in central areas of the three samples; B: 2400–3100 cm^{-1} region in which major peaks for collagen occur.

The frequency of the P–O stretch in the central areas of all three TT tympanic samples is almost identical at 960 ± 0.2 cm^{-1}. In each case, however, the peak position of the bioapatite at the edge of the bulla is higher than that of the center by >0.5 cm^{-1}, which is significant (Fig. 3 and Table 1). The differences in peak position reflect differences in the chemical environment of the phosphate between these apatite phases. The widths of the 960 cm^{-1} peaks indicate the degree of atomic order in the crystallites: the wider the peak, the more atomically disordered the material. For the central regions of all three tympanic bones, the full widths at half intensity (FWHM) of the deconvolved ~960 cm^{-1} band are almost identical, and they are wider than those for the edge (Table 1). In addition, of all three samples, the neonate has by far the narrowest FWHM value for its edge.

The 1070 cm^{-1} peak represents a combination of the ν_3 vibrational mode of PO_4^{3-} and the ν_1C–O stretching vibration of CO_3^{2-} [13,31,32,34,35]. The intensity of this peak indicates the degree of carbonate substitution for phosphate in bioapatite [13]. Within each transverse section, the position of this peak in the central areas is about 0.6 cm^{-1} lower with respect to edge areas (Table 1). More importantly, in all three samples, the normalized intensity (with respect to that of the 960 cm^{-1} P–O band) of the 1070 cm^{-1} peak is much stronger for the central areas than the edge region (Fig. 3A), indicating significantly higher carbonate contents in these central areas. Furthermore, the central area of the adult TT shows a slightly greater normalized intensity of its 1070 cm^{-1} peak (Fig. 3A) compared to the other samples, indicating that the highest carbonate concentrations occur in the mineral of the mature adult. No peaks are detected at 876 and 1105 cm^{-1} (Fig. 3A), which are the indicators of carbonate substitution for hydroxyl, confirming that most of the carbonate in the mineral substitutes for phosphate. The ratio of the areas of the 1070/960 peaks can be calculated to estimate carbonate contents based on our calibration against a suite of synthetic carbonated apatites analyzed in our group [35]. In all three bullae, the estimated carbonate contents on the edges are 2.1–2.6 wt.% lower than those in the central areas (Table 1). The carbonate contents both in the edges and in the central areas show an increase of ~1 wt.% in the progression from neonate to adult. In contrast, no prominent changes in carbonate are observed from the neonate to the sub-adult.

Edge areas are outer bands with a thickness of ~1 mm on all three sections. All edge materials show additional 1003 cm^{-1} and 2940 cm^{-1} peaks (Fig. 3B), indicative of an organic matrix, most of which is collagen in bone. A weak νC–C aromatic ring stretch at 1003 cm^{-1} is assigned to the phenylalanine component of collagen, and an envelope of peaks centered at about 2940 cm^{-1} can be assigned to specific C–H stretching vibrations within collagen or non-collagenous proteins [32,36]. These two sets of peaks occur in all normal bones [32,33,37]. In Fig. 3B, where all spectra are normalized to the intensity of the 960 cm^{-1} peak, the adult sample has the lowest intensity of the 2940 cm^{-1} peak, whereas the neonate and sub-adult have higher but similar intensities. Thus, the adult TT has the lowest concentration of organic matrix in its edge areas.

No peak is detected at 3570 cm^{-1} in any of the bullae, which is the indicator of hydroxyl in bioapatite. Any existing hydroxyl must be

Table 1
Positions of 960 cm^{-1} and 1070 cm^{-1} peaks of Raman spectra in three transverse sections (all units are cm^{-1}). Spectra of both central (dominant) and edge regions are included. FWHM of 960 cm^{-1} peak indicates degree of atomic order. Ratios (by area) of 1070/960 cm^{-1} peaks indicate CO_3^{2-} contents which are estimated based on calibration.

	Neonate		Sub-adult		Adult	
	Edge	Center	Edge	Center	Edge	Center
960 cm^{-1} position ($\pm$0.2 cm^{-1})	960.7	959.8	960.4	959.8	961.4	960.1
1070 cm^{-1} position ($\pm$0.2 cm^{-1})	1071.1	1071.8	1071.0	1071.5	1071.7	1072.3
960 cm^{-1} FWHM ($\pm$0.2 cm^{-1})	14.3	17.2	15.6	17.2	15.7	17.3
1070/960 cm^{-1} ($\pm$0.003)	0.229	0.319	0.223	0.330	0.262	0.377
Estimated wt.% CO_3^{2-}	6.7	8.8	6.6	9.0	7.5	10.1

below our detection limits, in part due to the broadening of the OH stretch as the carbonate content increases [38] and to an elevated background from slight fluorescence and from adsorbed water. This peak, however, can be detected for instance, in (also hypermineralized) enamel.

3.2. Carbon analysis

Coulometric bulk analysis of bullae (including central and edge material) yielded a TIC value of 1.62–1.87 wt.%. TIC is contributed primarily by carbonate in the bioapatite. Based on these TIC values, the calculated amount of carbonate (CO_3^{2-}) in the apatite is 8.10–9.35 wt.% (Table 2), which is above the range (5–8 wt.%) of carbonate contents in normal bone [12,13,39]. The carbonate content of the adult TT (9.35 wt.%) is also elevated compared to the ~8 wt.% value in the hypermineralized rostrum of the adult male MD whale [15] and the ~3.5 wt.% in enamel (only slightly more hypermineralized than the central bulla) [40].

Organic contents in bullae decrease with maturity. Among the three TT dolphin samples, the adult's bulla has the lowest TOC value. This relation is consistent with the Raman data, which show the adult to have the lowest concentration of organic matrix (based on the intensity of the 2940 cm^{-1} Raman peak). In addition, the bulla is not as hypermineralized in a bulk sample as the MD whale rostrum, as all three bullae show higher TOC values (>2 wt.%) than the rostrum (0.91 wt.%) (see Table 2). Collagen-enriched edges in the bullae would contribute most to such elevated organic contents.

Unexpectedly, the bulk TOC value increases during aging from the neonate to sub-adult, in apparent contradiction to the Raman results. The edge areas of the neonate bulla have an organic content similar to that of the sub-adult bulla based on the Raman analyses above. This apparent reversal in the trend for bulk TOC may be explained by the porosity of the neonate tissue, especially in the edge areas. In the neonate bulla, the central area is also porous compared to that of the two older samples; moreover, the neonate edge areas show a significantly higher porosity than the center. Thus, densification of the edge areas during aging may account for the elevated bulk TOC value in the adult compared to the neonate bulla.

3.3. Electron microprobe

Back-scattered-electron (BSE) images were taken of central and edge tissue of all three bullae. In these images (Fig. 4), darker colors indicate lighter elements; the latter typically are inferred to indicate the presence of collagen or vascular holes in the bone sections.

Table 2
Carbon analyses of three bullae. Carbonate (CO_3^{2-}) values were calculated from TIC. Data on the hypermineralized rostrum of an adult MD whale [15] are included for comparison.

	TC	TOC	TIC	Carbonate (wt.%)
Adult	3.92	2.06	1.87	9.35
Sub-adult	4.35	2.73	1.62	8.10
Neonate	3.78	2.16	1.62	8.10
Rostrum	2.49	0.91	1.57	7.88

Abundant vascular holes or voids occur in the central areas of the neonate section. The sub-adult and adult sections show abundant apparent fractures in the central areas that may have arisen from the process of thin-sectioning such highly mineralized tissue. However, the vascular holes or voids tend to be smaller in the central areas of the adult section (Fig. 4C) than in the other two samples.

BSE images of edge areas confirm the neonate bone to have the most porous structure (Fig. 4D). In addition, darker gray banding is present in the edge compared to the central areas of both sub-adult and adult sections, which indicates enrichment in organics, i.e., collagen.

A traverse of five equally spaced (~1.2 mm apart) EMP spot analyses was performed from each bulla's center to its outermost edge (see Fig. 2). The fifth spot in each sample is located in the edge area. Relatively homogeneous values of Ca/P atomic ratio and concentrations of Na, Mg, and other minor elements characterize the central areas (first four spots) within each sample (Table 3). The Ca/P atomic ratio of 1.7–1.8 in the bullae is higher than the 1.71 value of the rostrum and 1.63 of enamel, which had been analyzed previously by EMP [15]. The sum of the weight percents measured in the bullae is close to the ~87 wt.% value of the rostrum, but less than the ~94 wt.% for tooth enamel. Mg, S, and especially F concentrations are significantly lower in the bullae than those in the rostrum.

The neonate and sub-adult samples have a mass deficit of ~3–6% in the edge areas compared to their central areas, which is primarily due to the former's enrichment in collagen. In the adult bulla, the sum of the weight percents remains almost unchanged from the center to the edge (as slightly lower collagen content in the center compared to the edge was balanced by higher carbonate content in the bioapatite in the center). Furthermore, in all three samples, less Na is present in the edge compared to central areas. In the neonate and the sub-adult samples, Mg and S are also more abundant in edge areas, as collagen contains small amounts of Mg and S [15]. Ca/P ratios are almost constant between the edge and central areas in each of the three samples.

With respect to age, the total weight values of the edge areas increase ~5 wt.% from the neonate to adult. It is a decrease in the collagen in the edge of the bulla that mainly contributes to such change. In contrast, the total weight values in the central areas do not change (~87 wt.%) with age from neonate to adult. The Ca/P atomic ratios decrease slightly from neonate to sub-adult but then increase slightly from sub-adult to adult. This trend in the Ca/P ratio is the reverse of that for TOC, which was discussed above. In the compositional analyses of Table 3, Na's concentration demonstrates the greatest change during aging, increasing in both the central and edge areas. In the adult bulla, the Na, Mg, and S contents are almost identical between the edge areas and central areas. Additionally, the concentrations of Mg, S, and other minor elements (K, Cl, and F) remain constant in the central areas during aging, i.e., throughout all three samples.

4. Discussion

4.1. Center to edge: over-all

The bullae of dolphins have been studied as hypermineralized bone in zoological and biological contexts [1,2,4,6,41], but not as examples of

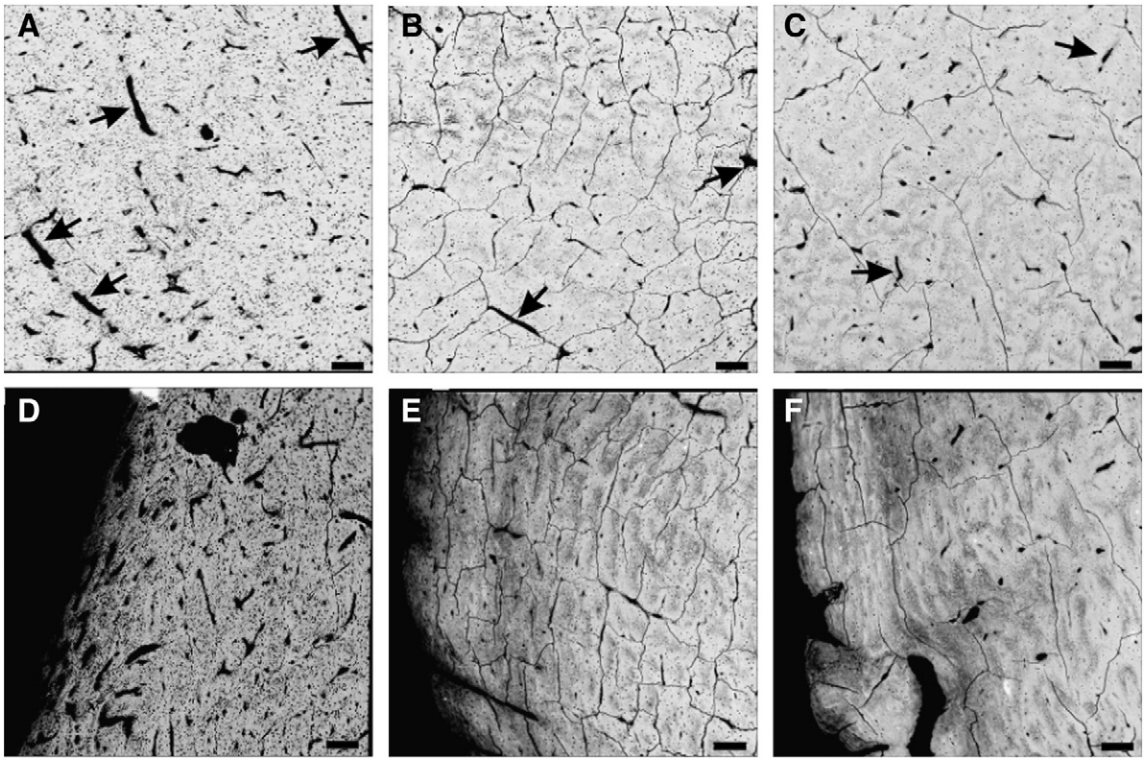

Fig. 4. Back-scattered-electron images of transverse sections. A, B, & C: Typical central areas of neonate, sub-adult, and adult. D, E, & F: Edge areas of neonate, sub-adult, and adult (scale bar = 200 μm). Arrows indicate vascular holes and voids in the sections.

bone mineral or its maturation. An important feature not addressed in the earlier literature is the difference between the volumetrically dominant regions of the bulla (central areas) and the millimeter-wide rims (edges) (Fig. 5). EMP results (see Table 3) show that the edges of the neonate and sub-adult have ~3–6% greater mass deficit than the central areas. Our Raman-based data on the carbonate concentration in bioapatite (Table 1) show these two bulla samples to have 2.1–2.4 wt.% less CO_3 in the edge compared to the central region. Therefore, the edge of the neonate and the sub-adult samples must contain ~5–8 wt.% more collagen than the central areas (to account for bulk carbon content). In contrast, the central areas have homogeneous mineral concentrations, which are close to those of the densest recoded bone — the hypermineralized rostrum (~96 wt.% mineral) of the adult male MD whale.

4.2. Center to edge: CO_3 and Na

The mineral of the bulla is CHAP throughout the edge and central areas, but the mineral is not compositionally identical throughout. The chemical environment is slightly different within the bioapatite (as shown by Raman) between edges and the central areas, especially for carbonate and sodium (as shown by EMP). Carbonate contents of ~9–10 wt.% in the central areas are significantly higher than the 6–7 wt.% values on the edges (see Table 1). Ca/P ratios (1.73–1.84) are higher than those in other hypermineralized bio-tissues, such as the rostrum and enamel, which appears to be due to greater amounts of CO_3^{2-} substitution for PO_4^{3-} in the bulla (see Formula (1)). Increased carbonate substitution usually leads to a lower degree of crystallinity in apatite [11,18,40,42]. As expected, the mineral in the edges (containing lower CO_3 concentration) shows a higher degree of crystallinity than the central areas, based on Raman spectroscopic evaluation of band widths. Na, which can substitute for Ca ions in apatite [15,40], is more abundant in the central areas of the bullae (Fig. 5).

4.3. During aging: over-all

During aging, the mineral concentration in the bulla did not increase significantly either in the central or edge areas, but the porosity was significantly reduced. This observation supports the proposal that the high density of the periotic and tympanic bullae results from almost complete filling of the inter-trabecular spaces with hypermineralized, embryonic, woven-fibered tissue. This mineralization process is different from that of the hypermineralized rostrum of the adult male whale *M. densirostris*, which undergoes hypermineralization during extensive remodeling and development of secondary osteons [1].

The adult bulla shows a mass deficit of <0.7 wt.% in the edge compared to central areas (Table 3). Additionally, Na, Mg and S concentrations are almost identical between the edge and central areas in the adult bulla. All other trace elements, K, Cl, and F, are extremely low in all three bullae and also do not significantly change with age. Therefore, from the neonate to adult, the contrast in the mineral concentrations between the edge and central areas decreases significantly (Fig. 6), i.e., the whole bulla becomes more homogeneous in mineral composition and mineral/matrix ratio with maturity.

4.4. During aging: CO_3 and Na

The carbonate contents increase slightly (~1 wt.%) in both the edge and central areas during aging (Table 1). The adult bulla is the bone with the highest carbonate content so far recorded, especially in the central areas (~10 wt.%). Enrichments in both CO_3^{2-} and Na in central areas coincide during aging. The substitution of carbonate for phosphate is known to be coupled with that of Na for Ca in bioapatites [11,15,17,43–47], which leads to co-incorporation of carbonate and sodium in bone. These coupled substitutions of CO_3^{2-} for PO_4^{3-} and Na^+ for Ca^{2+} account for the primary compositional change in the bioapatite of TT bullae during aging. The comparatively low and constant Na and CO_3 contents in the edge areas of the neonate and sub-adult suggest that

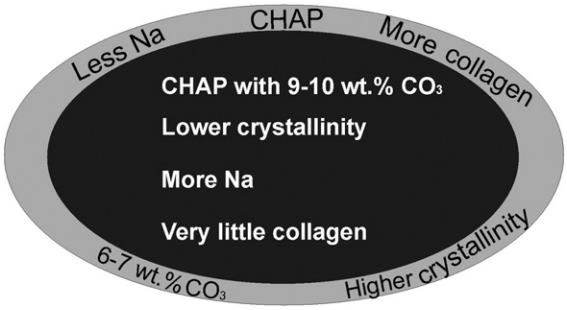

Fig. 5. A sketch of mineralogical and compositional contrast between the edge and central areas in the bulla (darker color = higher mineral content).

the edge areas are younger than the central areas. The substitution of most of the CO_3^{2-} for PO_4^{3-}, coupled with depletion of OH^- and Ca^{2+} in the bioapatite (Formula (1)), creates more vacant sites that are available for cation incorporation. Such coupled substitutions have also been documented in bioapatite within the rostrum of the MD male whale [15]. More specifically, the ratio of weight changes ΔNa_2O vs. ΔCO_3 from the neonate to adult is 1:2 (ΔNa_2O ~0.5 wt.% vs. ΔCO_3 ~1 wt.%, see Tables 3 and 1, respectively) in the central areas, which yields an atomic ratio of 1:1 for $\Delta Na/\Delta C$. A modified compositional model of the bioapatite in the bulla is therefore more appropriately described as:

$$Na_Y(Ca,Mg)_{10-x-Y}[(PO_4)_{6-x-Y}(CO_3)_{x+Y}](OH)_{2-x}. \quad (2)$$

Formula (2) is also applicable to the composition and compositional variation in normal bones, such as human bone, lamb femur, and elk antler, which have 0.8–0.9 wt.% Na_2O [15,17,40]. The lower Na contents in these normal bones, compared to the rostrum and bulla bones, are consistent with their lower carbonate contents.

4.5. During aging: sub-adult

The sub-adult sample does not show chemical properties intermediate between those of the neonate and the adult samples, e.g., carbonate contents (similar to the neonate), organic contents (similar to the neonate), and Ca/P ratios (lower than both the neonate and adult).

Table 3
EMP quantitative point analyses in neonate, sub-adult, and adult TT transverse sections (N = 5). The sum of the analyzed weight percents appears in the final column. Data from the rostrum [15] are shown for comparison. All values are in wt.% except for the Ca/P atomic ratios. Relative % errors are shown in parentheses.

	#	CaO	P_2O_5	Na_2O	MgO	SO_3	K_2O	Cl	F	Ca/P	Sum
Neonate	Center	50.20 (0.2)	34.62 (0.4)	1.28 (2)	0.43 (3)	0.15 (6)	0.05 (10)	0.03 (11)	0.04 (39)	1.84	86.78
		50.16 (0.2)	34.51 (0.4)	1.30 (2)	0.45 (3)	0.17 (6)	0.03 (13)	0.03 (12)	0.03 (44)	1.84	86.66
		50.69 (0.2)	35.56 (0.4)	1.33 (2)	0.46 (3)	0.18 (5)	0.05 (9)	0.03 (12)	0.02 (89)	1.80	88.30
		50.18 (0.2)	34.79 (0.4)	1.31 (2)	0.45 (3)	0.19 (5)	0.05 (9)	0.02 (15)	0.01 (107)	1.83	87.00
	Edge	47.80 (0.2)	32.94 (0.4)	1.13 (2)	0.50 (3)	0.21 (5)	0.04 (13)	0.06 (6)	0.02 (69)	1.84	82.67
Sub-adult	Center	50.02 (0.2)	35.39 (0.4)	1.55 (2)	0.40 (3)	0.18 (5)	0.08 (6)	0.04 (9)	0.03 (56)	1.79	87.67
		49.75 (0.2)	35.44 (0.4)	1.52 (2)	0.48 (3)	0.18 (5)	0.09 (6)	0.04 (10)	0.03 (44)	1.78	87.52
		49.87 (0.2)	35.68 (0.4)	1.52 (2)	0.46 (3)	0.21 (5)	0.08 (6)	0.03 (9)	0.03 (47)	1.77	87.87
		49.67 (0.2)	35.69 (0.4)	1.52 (2)	0.48 (3)	0.19 (5)	0.07 (6)	0.02 (9)	0.01 (90)	1.76	87.65
	Edge	47.17 (0.2)	34.01 (0.4)	1.18 (2)	0.71 (2)	0.32 (3)	0.05 (9)	0.03 (10)	0.00 (433)	1.73	84.80
Adult	Center	49.45 (0.2)	35.20 (0.4)	1.80 (2)	0.47 (3)	0.19 (5)	0.03 (15)	0.03 (10)	0.01 (236)	1.78	87.17
		50.16 (0.2)	35.05 (0.4)	1.78 (2)	0.45 (3)	0.16 (6)	0.03 (13)	0.04 (9)	0.05 (31)	1.81	87.69
		50.00 (0.2)	34.83 (0.4)	1.88 (2)	0.43 (3)	0.14 (6)	0.04 (13)	0.03 (11)	0.03 (43)	1.82	87.37
		50.09 (0.2)	34.79 (0.4)	1.82 (2)	0.46 (3)	0.18 (5)	0.04 (13)	0.02 (13)	0.04 (40)	1.82	87.41
	Edge	49.76 (0.2)	34.73 (0.4)	1.79 (2)	0.45 (3)	0.16 (6)	0.08 (6)	0.03 (11)	0.01 (39)	1.81	87.01
Rostrum		48.33	35.70	1.48	0.84	0.53	0.03	0.04	0.35	1.71	87.33

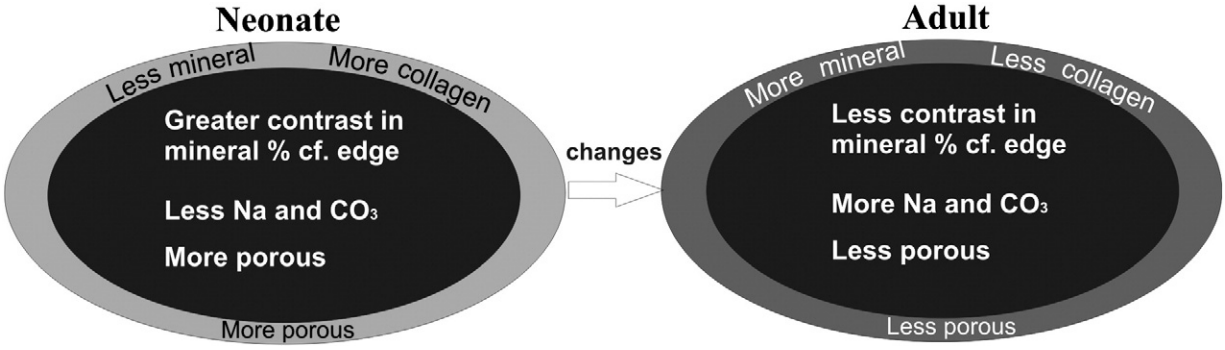

Fig. 6. A sketch of mineral content change in bullae during aging from the neonate to adult (darker color = higher mineral content).

However, the physical features of the sub-adult bulla, e.g., its degree of porosity, do have a status between those of the other two bullae. Therefore, the physical and chemical properties of bone may not change simultaneously in TT bullae. The results on the sub-adult (2.5 years) also suggest that in relatively long-lived animals, such short time intervals may not be sufficient for documenting the mineralogical changes in bone apatite with age, especially with regard to the chemical features.

4.6. Comparison with existing studies of bone aging

Changes in a number of chemical and physical properties of bone and its synthetic analogs have been traced over time. Mineralogical changes in CO_3 [16–18,20,22,23,48] and HPO_4^{2-} concentrations [20,49–52], Ca/P ratio [19,20,49], degree of crystallinity and crystal sizes [17–19,53], and mineral contents [16–19] during bone aging have been discussed in previous literature. Aging of synthetic apatite also has been studied [50,54,55] and provides an analog to bioapatite in bone. Although most scientists limited their research on maturity effects to a short time interval, ranging from days to a few years, a small number of studies analyzed bone samples over ranges of tens of years [17,18].

The high CO_3 and Na contents in the TT bullae compared to those in normal bones enabled the testing of a specific mechanism of co-inclusion of those two components within bone mineral. In contrast to the more than 1 wt.% increase in CO_3 over a period of 20 years in the dolphin bulla, there was an increase of only ~0.4 wt.% in human bone over a period of 90 years [17]. More importantly, a hypermineralized bone, such as the bulla, reduces the confounding effects from the presence of collagen and its entrained body fluid, thereby yielding relatively more accurate and precise chemical analyses [15].

The sodium ion has not attracted much interest in previous studies of bone mineral. Handschin and Stern [17] discovered an increase in Na_2O in human bone (0.76 to 0.82 wt.%) over the first 10 years of age, but this increase then halted. Increasing CO_3 concentration in bone mineral with age has been confirmed widely in human, bovine, and rat bones by Raman spectroscopy, infrared spectroscopy, carbon analysis, and other chemical analyses [16–18,20,21,23]. In the present study, carbonate contents in the TT bullae were assessed by three techniques, i.e., Raman spectroscopy, carbon analysis, and EMP — all of which gave consistent results — rather than a single technique, as in most previous studies.

Several studies reported a simultaneous increase in both the carbonate concentration and the degree of crystallinity in bone mineral with age [16,17,19]. In contrast, our study showed that the increase in carbonate concentration with age is not accompanied by a detectable change in the degree of crystallinity of the mineral in TT bullae as recorded by the constancy in Raman band width (see Table 1). Using X-ray diffraction and Raman spectroscopy, Yerramshetty et al. [18] discovered a similar lack of corresponding change in the crystallinity of human bones (from adults 52–85 years of age) as carbonate increased with age. They proposed that an increase in the size of the crystallites along the *c*-axis (inferred from X-ray diffraction) can counter-balance the size-diminishing effects from increasing carbonate. It was confirmed that the degree of crystallinity of bioapatite in bone does not increase continually, e.g., no appreciable variation in crystallinity (examined by X-ray diffraction) was identified within human bone after 30 years of age [17].

Kuhn et al. [19] studied the composition of bovine cortical bone aged 1–3 months to 4–5 years by EMP and coulometric analysis. They detected relatively constant (or slightly increasing) Ca/P and Ca/(P + C) atomic ratios of 1.61 vs. 1.64 and 1.39 vs. 1.41, respectively. Relatively constant Ca/P ratios were also identified in the bullae, although of higher value (~1.8).

The actual substitutional mechanisms of the incorporation of carbonate into bone mineral remain a subject of on-going research. Due to the difficulty of chemically analyzing the mineral in normal bone, much of this work has been done on synthetic analogs, some of which were precipitated from sodium-bearing solutions (as is the case in body fluids) and others in the absence of sodium. Several studies indicate a change in the nature of the carbonate substitution mechanism over certain compositional ranges, e.g., significant carbonate substitution for hydroxyl only at carbonate concentrations below 4 wt.% [56,57] and a change in the nature of the charge-balancing mechanism as carbonate concentrations exceed approximately 6.5 wt.%, which corresponds to one carbonate ion per unit cell [48]. The availability of non-pathologic hypermineralized bone samples may aid the development of carbonate substitution models that are consistent between synthetic and biological materials.

5. Conclusions

Selection of the hypermineralized dolphin's bulla permitted the monitoring of changes in the mineral/matrix ratio of bone, as well as compositional and crystallinity changes in bone mineral, over time in a long-lived mammal. The extremely low concentration of organics in the bulla enhanced the quality of the bone mineral analyses in that no chemical treatment for removal of collagen was needed. Moreover, use of spectroscopic and compositional point-analysis techniques (micrometer scale) enabled compositional–structural evaluation of the bone mineral at high spatial resolution. Such analysis is not possible in bone with normal concentrations of collagen.

Our research on the effect of aging on bone confirmed the intriguing coincidence of increasing CO_3 concentration with no apparent loss of crystallinity in the bioapatite. This coincidence is counterintuitive in that, when separately synthesized CHAP samples are compared, an increasing degree of carbonation correlates with a decreasing degree of crystallinity [7,18,20,42,58]. Further work on the bulla may reveal two or more independently operating processes that produce the unexpected carbonate–crystallinity trends documented during aging. One such process identified in this work is the coupling of the chemical

substitution of CO_3^{2-} for PO_4^{3-} with Na^+ for Ca^{2+} during aging. The importance of Na incorporation requires more attention in the study of how bone changes with age.

Several new findings relate to the nature of the bulla itself. The central volumetrically dominant areas of the bulla are clearly hypermineralized. However, the narrow edge areas have distinctly more collagen, and these two types of tissue should be differentiated in future research on the dolphin's bulla. Moreover, the entire bulla proceeds to become more homogeneous in mineral/collagen ratio and mineral chemistry during aging. Mineralogically, the question is whether we are recognizing the long-term approach to equilibrium between body fluid and mineral during aging. In addition, results from this study of the bulla, when coupled with our previous results on the whale rostrum [15,37], shed light on the nature of bioapatite in bone.

We recognize that the exceptionally high carbonate concentration in the bioapatite of the bulla excludes the latter's acceptance as "normal" bone. However, the rest of the chemistry of the bulla's bioapatite and the nature of its compositional variations support its use as a bone-apatite model. Indeed, the fact that the bulla's bioapatite composition ranges up to higher values for some essential components, e.g., CO_3 and Na, than in typical bone has made more clear an important element-incorporation mechanism in bone. Investigation of these mechanisms is especially important in the on-going research to understand the process of aging in bone and the possible effects of mineral composition on the degradation of bone properties that occurs in osteoporosis and osteopetrosis [59–62]. The amenability of dolphin bullae in this study to detailed, spatially resolved chemical and Raman spectroscopic analysis supports the undertaking of future analysis of multiple suites of bullae of well-estimated ages.

Role of the funding sources

The funding sources had no involvement in study design, sample collection, analysis or interpretation of data, writing, or the decision to submit the article for publication.

Acknowledgements

This work was partially funded by NIH R01 AR055580 and NSF CAREER 844607. We thank Charles Potter for the USNM bulla samples and for information on the biology and habits of the dolphin *T. truncates*. We appreciate Paul Carpenter's assistance with electron microprobe analyses. We thank Prof. Daniel Hirmas for the carbon analyses and Dr. Stavros Thomopoulos and Dr. Guy Genin for discussions on biomineralization and bioapatite. Comments by two anonymous reviewers were also much appreciated.

References

[1] V. de Buffrénil, W. Dabin, L. Zylberberg, Histology and growth of the cetacean petrotympanic bone complex, J. Zool. 262 (2004) 371–381.
[2] S. Nummela, T. Wagar, S. Hemila, T. Reuter, Scaling of the cetacean middle ear, Hear. Res. 133 (1999) 71–81.
[3] D.R. Ketten, Cetacean ears, in: W.W.L. Au, A.N. Popper, R.R. Fay (Eds.), Hearing by Whales and Dolphins, Springer, New York, 2000, pp. 43–108.
[4] S. Nummela, T. Reuter, S. Hemila, P. Holmberg, P. Paukku, The anatomy of the killer whale middle ear (*Orcinus orca*), Hear. Res. 133 (1999) 61–70.
[5] M. Yamato, D.R. Ketten, J. Arruda, S. Cramer, K. Moore, The auditory anatomy of the minke whale (*Balaenoptera acutorostrata*): a potential fatty sound reception pathway in a Baleen whale, Anat. Rec. 295 (2012) 991–998.
[6] T.W. Cranford, P. Krysl, M. Amundin, A new acoustic portal into the Odontocete ear and vibrational analysis of the tympanoperiotic complex, PLoS One 5 (2012) 1–29.
[7] J.C. Elliott, Calcium phosphate biominerals, in: M.J. Kohn, J. Rakovan, J.M. Hughes (Eds.), Phosphates: Geochemical, Geobiological, and Materials Importance, Reviews in Mineralogy and Geochemistry, vol. 48, Mineralogical Society of America, Chantilly, Virginia, 2002, pp. 427–453.
[8] C. Rey, C. Combes, C. Drouet, A. Lebugle, H. Sfihi, A. Barroug, Nanocrystalline apatites in biological systems: characterisation, structure and properties, Mater. Werkst. 38 (2007) 996–1002.
[9] J.D. Pasteris, C.H. Yoder, B. Wopenka, Molecular water in nominally unhydrated carbonated hydroxylapatite: the key to a better understanding of bone mineral, Am. Mineral. 99 (2014) 16–27.
[10] G.Y. Cho, Y.T. Wu, J.L. Ackerman, Detection of hydroxyl ions in bone mineral by solid-state NMR spectroscopy, Science 300 (2003) 1123–1127.
[11] J.C. Elliott, Fluorapatite and chlorapatite, in: J.C. Elliott (Ed.), Structure and Chemistry of the Apatites and Other Calcium Orthophosphates, Elsevier, The Netherlands, 1994, pp. 63–104.
[12] S.V. Dorozhkin, M. Epple, Biological and medical significance of calcium phosphates, Angew. Chem. 41 (2002) 3130–3146.
[13] G. Penel, G. Leroy, C. Rey, E. Bres, MicroRaman spectral study of the PO_4 and CO_3 vibrational modes in synthetic and biological apatites, Calcif. Tissue Int. 63 (1998) 475–481.
[14] L.D. Mkukuma, J.M. Skakle, I.R. Gibson, C.T. Imrie, R.M. Aspden, D.W. Hukins, Effect of the proportion of organic material in bone on thermal decomposition of bone mineral: an investigation of a variety of bones from different species using thermogravimetric analysis coupled to mass spectrometry, high-temperature X-ray diffraction, and Fourier transform infrared spectroscopy, Calcif. Tissue Int. 75 (2004) 321–328.
[15] Z. Li, J.D. Pasteris, Chemistry of bone mineral, based on the hypermineralized rostrum of the beaked whale *Mesoplodon densirostris*, Am. Mineral. (2014), http://dx.doi.org/10.2138/am.2014.4571 (in press).
[16] A.L. Boskey, R. Coleman, Aging and bone, J. Dent. Res. 89 (2010) 1333–1348.
[17] R.G. Handschin, W.B. Stern, X-ray diffraction studies on the lattice perfection of human bone apatite (Crista iliaca), Bone 16 (1995) 355S–363S.
[18] J.S. Yerramshetty, C. Lind, O. Akkus, The compositional and physicochemical homogeneity of male femoral cortex increases after the sixth decade, Bone 39 (2006) 1236–1243.
[19] L.T. Kuhn, M.D. Grynpas, C.C. Rey, Y. Wu, J.L. Ackerman, M.J. Glimcher, A comparison of the physical and chemical differences between cancellous and cortical bovine bone mineral at two ages, Calcif. Tissue Int. 83 (2008) 146–154.
[20] C. Rey, C. Combes, C. Drouet, H. Sfihi, A. Barroug, Physico-chemical properties of nanocrystalline apatites: implications for biominerals and biomaterials, Mater. Sci. Eng. C 27 (2007) 198–205.
[21] E. Donnelly, A.L. Boskey, S.P. Baker, M.C. van der Meulen, Effects of tissue age on bone tissue material composition and nanomechanical properties in the rat cortex, J. Biomed. Mater. Res. 92 (2009) 1048–1056.
[22] C. Rey, V. Renugopalakrishnan, B. Collins, M.J. Glimcher, Fourier transform infrared spectroscopic study of the carbonate ions in bone mineral during aging, Calcif. Tissue Int. 49 (1991) 251–258.
[23] L.M. Miller, W. Little, A. Schirmer, F. Sheik, B. Busa, S. Judex, Accretion of bone quantity and quality in the developing mouse skeleton, J. Bone Miner. Res. 22 (2007) 1037–1045.
[24] L.M. Miller, V. Vairavamurthy, M.R. Chance, R. Mendelsohn, E.P. Paschalis, F. Betts, A. L. Boskey, In situ analysis of mineral content and crystallinity in bone using infrared micro-spectroscopy of the ν(4) PO_4^{3-} vibration, BBA-Gen Sub 1527 (2001) 11–19.
[25] J.S. Nyman, A. Roy, X.M. Shen, R.L. Acuna, J.H. Tyler, X.D. Wang, The influence of water removal on the strength and toughness of cortical bone, J. Biomech. 39 (2006) 931–938.
[26] P.A. Timmins, J.C. Wall, Bone water, Calcif. Tissue Res. 23 (1977) 1–5.
[27] M.C. Mattson, K.D. Mullin, G.W. Ingram, W. Hoggard, Age structure and growth of the bottlenose dolphin (*Tursiops truncatus*) from strandings in the Mississippi sound region of the north-central Gulf of Mexico from 1986 to 2003, Mar. Mamm. Sci. 22 (2006) 654–666.
[28] E.E. Engleman, L.L. Jackson, D.R. Norton, Determination of carbonate carbon in geological-materials by coulometric titration, Chem. Geol. 53 (1985) 125–128.
[29] D.R. Hirmas, B.F. Platt, S.T. Hasiotis, Determination of calcite and dolomite content in soils and paleosols by continuous coulometric titration, Soil Sci. Soc. Am. J. 76 (2012) 1100–1106.
[30] L.L. Jackson, S.R. Roof, Determination of the forms of carbon in geologic materials, Geostand. Newslett. 16 (1992) 317–323.
[31] A. Awonusi, M.D. Morris, M.M. Tecklenburg, Carbonate assignment and calibration in the Raman spectrum of apatite, Calcif. Tissue Int. 81 (2007) 46–52.
[32] G. Penel, C. Delfosse, M. Descamps, G. Leroy, Composition of bone and apatitic biomaterials as revealed by intravital Raman microspectroscopy, Bone 36 (2005) 893–901.
[33] B. Wopenka, A. Kent, J.D. Pasteris, Y. Yoon, S. Thomopoulos, The tendon-to-bone transition of the rotator cuff: a preliminary Raman spectroscopic study documenting the gradual mineralization across the insertion in rat tissue samples, J. Appl. Spectrosc. 62 (2008) 1285–1294.
[34] O. Akkus, F. Adar, M.B. Schaffler, Age-related changes in physicochemical properties of mineral crystals are related to impaired mechanical function of cortical bone, Bone 34 (2004) 443–453.
[35] J.D. Pasteris, B. Wopenka, S. Man, Concerning the cause of the 1070 Δcm^{-1} Raman band in carbonated apatite, Abstract for 8th Biomaterials Congress, 2008, p. A478.
[36] H.G. Edwards, D.W. Farwell, J.M. Holder, E.E. Lawson, Fourier-transform Raman spectra of ivory. III: Identification of mammalian specimens, Spectrochim. Acta A 53A (1997) 2403–2409.
[37] Z. Li, J.D. Pasteris, D. Novack, Hypermineralized whale rostrum as the exemplar for bone mineral, Connect. Tissue Res. 54 (2013) 167–175.
[38] J.D. Pasteris, C.H. Yoder, M.P. Sternlieb, S. Liu, Effect of carbonate incorporation on the hydroxyl content of hydroxylapatite, Mineral. Mag. 76 (2012) 2741–2759.
[39] H. Ou-Yang, E.P. Paschalis, W.E. Mayo, A.L. Boskey, R. Mendelsohn, Infrared microscopic imaging of bone: spatial distribution of CO_3^{2-}, J. Bone Miner. Res. 16 (2001) 893–900.
[40] R.Z. LeGeros, J. LeGeros, Phosphate minerals in human tissues, in: J.O. Nriagu, P.B. Moore (Eds.), Phosphate Minerals, Springer, New York, 1984, pp. 351–384.

[41] W.W.L. Au, A.N. Popper, R.R. Fay, Cetacean Ears, Springer, New York, 2000.
[42] R.Z. LeGeros, R. Kijkowska, C. Bautista, J.P. LeGeros, Synergistic effects of magnesium and carbonate on properties of biological and synthetic apatites, Connect. Tissue Res. 32 (1995) 525–531.
[43] S.M. Barinov, I.V. Fadeeva, D. Ferro, J.V. Rau, S.N. Cesaro, V.S. Komlev, A.S. Fomin, Stabilization of carbonate hydroxyapatite by isomorphic substitutions of sodium for calcium, Russ. J. Inorg. Chem. 53 (2008) 164–168.
[44] S. Cazalbou, C. Combes, D. Eichert, C. Rey, Adaptative physico-chemistry of bio-related calcium phosphates, J. Mater. Chem. 14 (2004) 2148–2153.
[45] G. Daculsi, J.M. Bouler, R.Z. LeGeros, Adaptive crystal formation in normal and pathological calcifications in synthetic calcium phosphate and related biomaterials, Int. Rev. Cytol. 172 (1997) 129–189.
[46] S. Peroos, Z.M. Du, N.H. de Leeuw, A computer modelling study of the uptake, structure and distribution of carbonate defects in hydroxy-apatite, Biomaterials 27 (2006) 2150–2161.
[47] R.Z. LeGeros, Apatites in biological-systems, Prog. Cryst. Growth Charact. 4 (1981) 1–45.
[48] J.D. McElderry, P. Zhu, K.H. Mroue, J. Xu, B. Pavan, M. Fang, G. Zhao, E. McNerny, D.H. Kohn, R.T. Franceschi, M.M. Holl, M.M. Tecklenburg, A. Ramamoorthy, M.D. Morris, Crystallinity and compositional changes in carbonated apatites: evidence from P solid-state NMR, Raman, and AFM analysis, J. Solid State Chem. 206 (2013).
[49] R. Legros, N. Balmain, G. Bonel, Age-related changes in mineral of rat and bovine cortical bone, Calcif. Tissue Int. 41 (1987) 137–144.
[50] Y.T. Wu, J.L. Ackerman, H.M. Kim, C. Rey, A. Barroug, M.J. Glimcher, Nuclear magnetic resonance spin–spin relaxation of the crystals of bone, dental enamel, and synthetic hydroxyapatites, J. Bone Miner. Res. 17 (2002) 472–480.
[51] I.A. Karampas, M.G. Orkoula, C.G. Kontoyannis, Effect of hydrazine based deproteination protocol on bone mineral crystal structure, J. Mater. Sci. Mater. Med. 23 (2012) 1139–1148.
[52] D. Farlay, G. Panczer, C. Rey, P.D. Delmas, G. Boivin, Mineral maturity and crystallinity index are distinct characteristics of bone mineral, J. Bone Miner. Metab. 28 (2010) 433–445.
[53] C. Meneghini, M.C. Dalconi, S. Nuzzo, S. Mobilio, R.H. Wenk, Rietveld refinement on X-ray diffraction patterns of bioapatite in human fetal bones, Biophys. J. 84 (2003) 2021–2029.
[54] E.D. Eanes, J.L. Meyer, The maturation of crystalline calcium phosphates in aqueous suspensions at physiologic pH, Calcif. Tissue Res. 23 (1977) 259–269.
[55] S. Rollin-Martinet, A. Navrotsky, E. Champion, D. Grossin, C. Drouet, Thermodynamic basis for evolution of apatite in calcified tissues, Am. Mineral. (2013) 2037–2045.
[56] J. Barralet, S. Best, W. Bonfield, Carbonate substitution in precipitated hydroxyapatite: an investigation into the effects of reaction temperature and bicarbonate ion concentration, J. Biomed. Mater. Res. 41 (1998) 79–86.
[57] D.G. Nelson, J.D. Featherstone, Preparation, analysis, and characterization of carbonated apatites, Calcif. Tissue Int. 34 (Suppl. 2) (1982) S69–S81.
[58] M.J. Glimcher, Bone: nature of the calcium phosphate crystals and cellular, structural, and physical chemical mechanisms in their formation, in: N. Sahai, M.A.A. Schoonen (Eds.), Medical Mineralogy and Geochemistry, Reviews in Mineralogy and Geochemistry, vol. 64, Mineralogical Society of America, Washington, D.C., 2006, pp. 223–282.
[59] M. Aref, M.A. Gallant, J.M. Organ, J.M. Wallace, C.L. Newman, D.B. Burr, D.M. Brown, M.R. Allen, In vivo reference point indentation reveals positive effects of raloxifene on mechanical properties following 6 months of treatment in skeletally mature beagle dogs, Bone 56 (2013) 449–453.
[60] J.C. Burket, D.J. Brooks, J.M. MacLeay, S.P. Baker, A.L. Boskey, M.C. van der Meulen, Variations in nanomechanical properties and tissue composition within trabeculae from an ovine model of osteoporosis and treatment, Bone 52 (2013) 326–336.
[61] S. Gourion-Arsiquaud, L. Lukashova, J. Power, N. Loveridge, J. Reeve, A.L. Boskey, Fourier transform infrared imaging of femoral neck bone: reduced heterogeneity of mineral-to-matrix and carbonate-to-phosphate and more variable crystallinity in treatment-naive fracture cases compared with fracture-free controls, J. Bone Miner. Res. 28 (2013) 150–161.
[62] A. Boskey, Mineral changes in osteopetrosis, Crit. Rev. Eukaryot. Gene 13 (2003) 109–116